Tumor Response Estimation Algorithm for Radar-based Microwave Breast Cancer

Douglas Kurrant[1], Jeff Sill[1], Elise Fear[1],
[1]Dept. of Elect. & Comp. Engineering, Schuilich School Engineering, University of Calgary, Canada fear@ucalgary.ca

Abstract

A considerable challenge for the successful implementation of the radar-based breast cancer detection techniques is the reduction of clutter. In this paper, a previously proposed clutter reduction algorithm is modified and applied to numerical data generated with realistic breast models. Its ability to estimate a tumor response contained in the data for these more complex cases is demonstrated.

1. Introduction

We are developing tissue sensing adaptive radar (TSAR) for early stage breast cancer detection. The aim of this method, like the other radar-based imaging techniques, is to identify sources of backscattered energy arising from the dielectric property differences between the various breast tissues. An antenna is used to illuminate the breast with low power, ultra-wideband pulses of microwave energy. The scattered fields (or reflections) are received at the same antenna. The antenna is sequentially moved around the breast in a 3D pattern in order to collect reflections at multiple locations.

The scattered fields received at each antenna contain early and late-time contributions. Algorithms are used to pre-condition the signals in order to remove the antenna reverberations, and reflections from the skin-breast interface that are contained in the early-time scattered fields [1]. The late-time fields that remain contain backscatter from a possible lesion (the tumor response) and clutter. In this context, clutter is defined as signals arising from scattering mechanisms other than the tumor. Effective suppression of the clutter is required in order to successfully detect and localize tumors.

A feature extraction technique using a piecewise parametric function to model the tumor response contained in the late-time scattered fields was presented in [2]. The method was incorporated into a pattern classification algorithm in [3] and applied to both simulated and experimental data generated using simple cylindrical breast models. In this paper the algorithm is extended so that it may be applied to numerical data generated from magnetic resonance (MR) image-derived three-dimensional (3D) breast models that are more realistic in terms of size, shape, electrical properties, and tissue distribution.

2.1 Models

We examine data collected with a realistic breast model based on MR images and simulated with the finite difference time domain (FDTD) method. Two 3D breast models are constructed by segmenting MR images as described in [4]. Specialized hardware cards (Acceleware, Calgary, AB) are then used to run FDTD simulations of these complex models. The breast model is illuminated with a resistively loaded Wu-King dipole as in [1]. The antenna is excited with a differentiated Gaussian waveform with a center frequency of 4.0 GHz and a full width half maximum of 1.4 – 8.7 GHz. Reflections are recorded as the antenna is moved to 160 different positions around the breast in order to construct a *5 x 32* synthetic antenna array.

In the first model, the interior of the breast is identified and then filled with homogeneous fatty tissue having electromagnetic properties of $\varepsilon_r = 9$, $\sigma = 0.4$ S/m. A 2-mm layer of skin with electromagnetic properties of $\varepsilon_r = 36$, $\sigma = 4$ S/m is placed around the model. Glandular tissue is included using a simple thresholding technique [4] that assigns electromagnetic properties of $\varepsilon_r = 16$, $\sigma = 1$ S/m to those pixel intensities of the MR image that exceed a pre-selected threshold. Finally, a 6-mm diameter spherical tumor with $\varepsilon_r = 50$, $\sigma = 4$ S/m is added to the breast model. We call this the *simple glandular* model. A 2D representation of this model is shown in Figure 1a.

The second model is constructed with a technique described by [5]. The interior of the breast is established and filled with homogeneous fatty tissue with $\varepsilon_r = 9$, $\sigma = 0.4$ S/m. Once the glandular tissue is identified, a linear function is used to map the MR pixel intensity to the electromagnetic properties of the glandular tissue. The pixel intensities between the minimum and the maximum values are linearly mapped to the interval of electromagnetic properties [($\varepsilon_r = 15.2$, $\sigma = 1.7$

S/m), (ε_r = 27.5, σ = 3.0 S/m)]. A 2-mm thick skin layer and a 6-mm spherical tumor are then added. We call this the *bimodal* model and show it in Figure 1b. We note that the electrical properties of both models do not incorporate frequency dispersion. Nevertheless, the models provide a reasonable test-bed for the initial development of the clutter reduction algorithms.

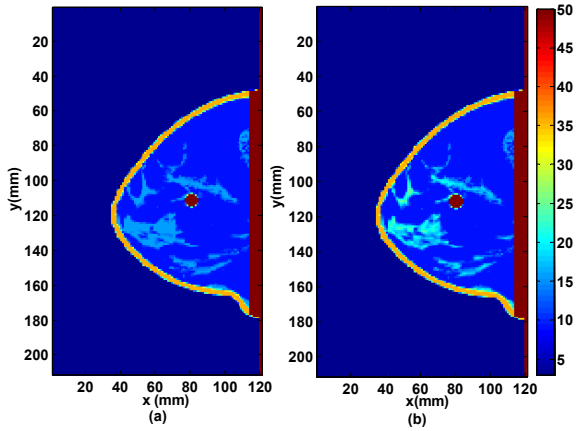

Fig. 1: Numerical breast models with the tumor located at (80, 110) (a) Simple glandular (b) Bimodal.

2.2 Signal Processing

The signals received by each antenna are pre-conditioned to remove the early-time response by subtracting signals recorded without the breast model present. The pre-conditioned signal for each element in the synthetic antenna array is modeled as,

$$x(n) = t(n) + c(n) + w(n),\ n = 0, \ldots, N-1 \qquad (1)$$

where $t(n)$ represents the contributions from the tumor, $c(n)$ represents the clutter contributions, $w(n)$ represents additive white Gaussian noise, and N is the duration of the received signal. A piecewise time-domain parametric function introduced in [3], is used to model the tumor response in Equation (1), and is given by,

$$t(n) = \begin{cases} A t_\alpha(n - t_d), & n = 0, \ldots, t_d \\ A e^{-n\gamma} t_\alpha(n - t_d), & n = t_d, \ldots, N-1 \end{cases} \qquad (2)$$

where A is a time independent scaling factor, $t_\alpha(n)$ is a tumor reference response, t_d is the time delay between the actual tumor response and the reference signal, and γ is a damping factor. For this work, a set of four reference signatures is constructed using finite difference time domain (FDTD) simulations [6]. A Bayesian estimation technique using a maximum *a posteriori* probability (MAP) approach developed in [3] is used to estimate the value of each parameter in (2), and is given by,

$$\theta_{map} = \arg\left[\max_{\theta} \left\{ J(\theta),\ \forall \alpha \in \Lambda,\ \forall t_d \in T_d \right\} \right], \qquad (3)$$

where $J(\theta)$ is a cost function which implies the match between the information contained in the signal and a tumor response. A feature extraction algorithm described in [2] segments the pre-processed signal received at a selected antenna into multiple overlapping windows. The MAP given by Equation (3) is applied to the signal contained within each window to evaluate estimates of the function parameters and stores the estimates as a feature vector. At the termination of the algorithm, a number of feature vectors for prospective tumor estimate candidates have been constructed and stored for further evaluation. Typically, high cost function values are obtained for more than one window. Hence ambiguity exists as to which one of the feature vectors is likely to correspond to an actual tumor. A pattern classification algorithm is used to resolve this ambiguity.

An illustration of the classification algorithm for a typical synthetic antenna array is shown in Figure 2. The aim of the classification procedure is to determine which feature vector of each antenna corresponds to a tumor response. The classification algorithm was initially designed and tested on a simple cylindrical breast model [3,7]. In order to

accommodate the more realistic breast models, the classification procedure is successively applied to the antenna array. The algorithm is initialized by selecting the antenna with the highest peak cost function value above a pre-determined threshold, which implies that a tumor response has possibly been received by the antenna. Once the antenna is found, a *3 x 3* spatial window is formed with the antenna at the center. Each of the neighboring antennas within the window is examined to determine if a similar tumor response has been received. If all of the antennas within the initialization window satisfy these criteria, then the spatial window is expanded to form an *n x 3* array of antenna elements. The vectors in each column of the spatial window are then classified. The classification procedure continues by adding columns for classification until all of the vectors have been classified.

To accommodate the detection of multiple targets, the classification procedure is repeated by searching the antenna array for the next antenna with a cost function value above a pre-determined threshold. After selecting the antenna, spatial windows having *3 x 1* and *1 x 3* antenna elements are formed with the antenna at the center. This initialization step is used to accommodate a weaker tumor response. If all of the antennas within either of the two initialization windows have detected a tumor response within a pre-determined time-of-arrival window width, then the initialization vectors are examined to determine if they have already been classified. If the vectors have already been classified, then the initialization is repeated for the next highest peak cost function value. Otherwise, the classification process is repeated. The classification process for the second iteration is terminated once a set of initialization vectors cannot be found and none of the antennas have a cost function value above a pre-determined threshold.

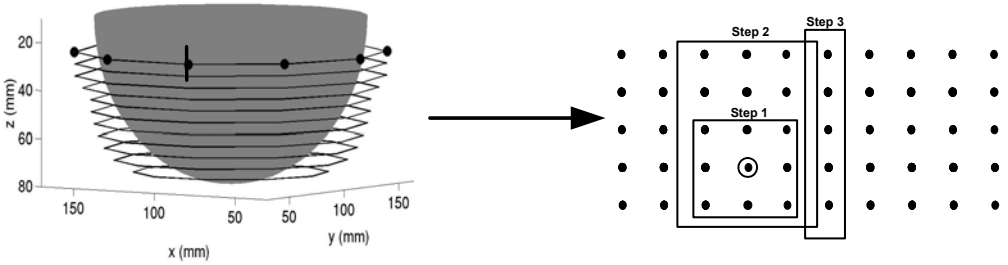

Fig. 2: An illustration of the classification process.

At the termination of the classification algorithm, the feature vectors associated with a tumor response are stored in an array. An estimated tumor response is constructed using the tumor response model given by Equation (1) and the focusing algorithm described by [1] is applied to the array of tumor response estimates in order to create an image.

3. Results

The performance of the algorithm when applied to the data is evaluated first by providing a single-signal analysis. We examine the peak value of the cost function (ρ_{max}), the cross-correlation between the actual target response and the target estimate ($r_{\hat{t}t}$), and the distance error between the actual target response and the target estimated. The proportion of responses detected is also examined. The results are recorded in Table 1.

Model	ρ_{max}	$r_{\hat{t}t}$	Distance Error (mm)	Responses detected (%)
Simple glandular	0.88	0.89	1.44	26
Bimodal	0.78	0.82	0.62	14

Table 1: Single-signal analysis results. The averages are computed over the responses detected.

The results in Table 1 indicate that the average cost function value and the proportion of tumor responses detected were larger for the simple glandular model. This reflects the more challenging problem of detecting a tumor response in the bimodal model. Nevertheless, the average cross-correlation is comparable and the average distance error is better for the bimodal model case. This implies that the tumor response, once detected, is estimated by the algorithm equally well as the breast model increases in complexity. Next, images are formed from the tumor estimates for the synthetic antenna array using the time-shift-and-sum focusing algorithm in [1]. The focusing algorithm is applied to the data using average breast tissue permittivity values. The images are created with the inclusion of the algorithm developed by Williams *et. al* [8] that reconstructs an estimate of the surface of the model from the information received by the antennas. The images are normalized to the peak value of the data and the pixel intensity corresponds to backscattered energy.

We note that the tumor is not detected in either model without the inclusion of the feature extraction/classification algorithm. Conversely, with the inclusion of the algorithm, the simple time-shift-and sum focusing algorithm was sufficient to provide detection and localization. The images for the bimodal modal are shown in Figure 3. We observe that a second prominent artifact is present in the coronal view. The artifact is primarily due to the excitation signal used and the small number of antennas that sensed the tumor response. The use of a different excitation signal is expected to improve the image results.

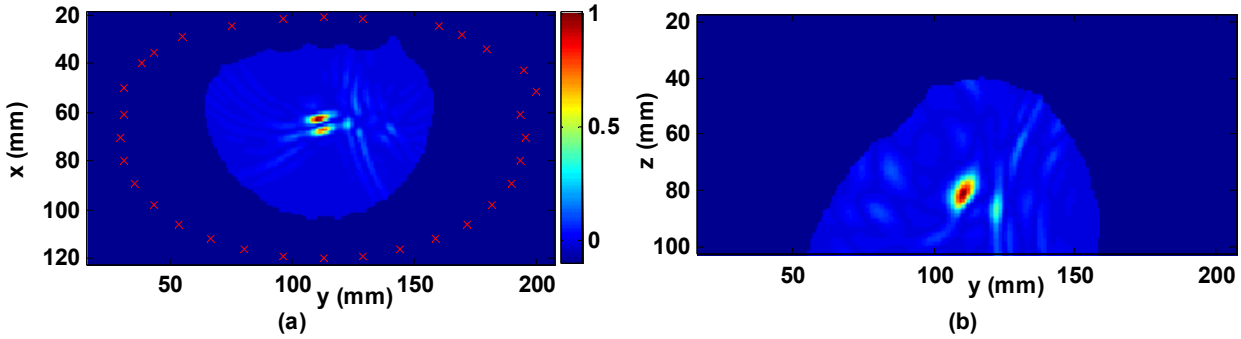

Fig 3: Images for the bimodal model showing the tumor response for (a) coronal view, and (b) sagittal view. The tumor was estimated to be located at x = 63, y = 110, and z = 80 mm while the actual tumor location is x = 60, y = 110, and z = 80 mm.

4. Conclusion

In this paper we used a feature extraction/classification algorithm to detect and estimate the tumor response in data generated from two different realistic 3D numerical breast models developed from MR images. The single-signal results indicate that the challenge of detecting the tumor response increases with the complexity of the model. However, the increase in complexity of the models did not adversely affect the performance of the algorithm to accurately estimate the tumor response. These preliminary results demonstrate that the algorithm may be incorporated into the TSAR algorithm to allow 3D tumor localization to be achieved.

5. References

[1] J.M. Sill and E.C Fear, "Tissue Sensing Adaptive Radar for Breast Cancer Detection and Experimental Investigation of Simple Tumor Models," *IEEE Trans. Microwave Theory Tech.*, vol. 53, pp. 3312–3319, Nov. 2005.

[2] D.J. Kurrant, E.C. Fear, and D.T. Westwick, "Tumor Estimation in Tissue Sensing Adaptive Radar (TSAR) Signals," *in 20th Canadian Conf. on Elect. and Comp. Eng.*, pp. 860–863, Vancouver, B.C., April 22-26 2007.

[3] D.J. Kurrant, E.C. Fear, and D.T. Westwick, "Tumor Response Estimation in Radar-based Microwave Breast Cancer Detection," *IEEE Trans. Biomed. Eng.*, accepted Jan 2008.

[4] J.M. Sill, T.C. Williams, E.C. Fear, R. Frayne, M. Okoniewski, "Realistic Breast Models for Second Generation Tissue Sensing Adaptive Radar System", *EUCAP*, Nov 8, 2007.

[5] M.Converse, E.J.Bond, B.D.Van Veen and S.C.Hagness,"A Computational Study of Ultra-Wideband Microwave Hyperthermia for Breast Cancer Treatment," *IEEE Trans. Microwave Theory Tech.*, vol. 54, pp. 2169–2180, May 2006.

[6] E.C. Fear, X. Li, S.C. Hagness, and M.A. Stuchly, "Confocal Microwave Imaging for Breast Cancer Detection: Localization of Tumors in Three Dimensions," *IEEE Trans. Biomed. Eng.*, vol. 49, pp. 812–822, Aug. 2002.

[7] J.M. Sill and E.C Fear, "Tissue Sensing Adaptive Radar for Breast Cancer Detection: Study of Immersion Liquids," *Electron. Lett.*, vol. 41 no. 3, pp. 113–115, Feb. 2005.

[8] T.C. Williams, and E.C. Fear "Breast Surface Estimation for Radar-Based Breast Imaging Systems" *IEEE Trans. Microwave Theory Tech.*, vol. 54, no.4, pp. 1308–1314, April 2006.